Journal of Advanced Research 47 (2023) 41–56

Contents lists available at ScienceDirect

Journal of Advanced Research

journal homepage: www.elsevier.com/locate/jare

Original Article

ANGPTL8 accelerates liver fibrosis mediated by HFD-induced inflammatory activity via LILRB2/ERK signaling pathways

Zongli Zhang [a,b,1], Yue Yuan [a,d,1], Lin Hu [a,b,1], Jian Tang [a,b], Zhongji Meng [e], Longjun Dai [f], Yujiu Gao [a,b], Shinan Ma [a], Xiaoli Wang [a], Yahong Yuan [a], Qiufang Zhang [a], Weibin Cai [c,g,*], Xuzhi Ruan [a,b,*], Xingrong Guo [a,b,*]

[a] Institute of Pediatric Disease, Hubei Key Laboratory of Embryonic Stem Cell Research, School of Basic Medical Sciences, Taihe Hospital, Hubei University of Medicine, Shiyan, Hubei 442000, China
[b] Department of Neurosurgery, Hubei Clinical Research Center for Umbilical Cord Blood Hematopoietic Stem Cells, Taihe Hospital, Hubei University of Medicine, Shiyan 442000, Hubei, China
[c] Guangdong Engineering & Technology Research Center for Disease-Model Animals, Laboratory Animal Center, Zhongshan School of Medicine, Sun Yat-sen University, Guangzhou 510080, Guangdong, China
[d] College of Pharmacy, Hubei University of Medicine, Shiyan, Hubei 442000, China
[e] Hubei Clinical Research Center for Precise Diagnosis and Treatment of Liver Cancer, Shiyan, Hubei 442000, China
[f] Department of Neurosurgery, Taihe Hospital, Hubei University of Medicine, Shiyan, Hubei 442000, China
[g] Department of Biochemistry, Zhongshan School of Medicine, Sun Yat-sen University, Guangzhou 510080, Guangdong, China

HIGHLIGHTS

- The expression level of ANGPTL8 is correlated with liver fibrosis staging.
- ANGPTL8 knockout suppresses HFD-induced hepatic steatosis and liver fibrosis in mice.
- ANGPTL8 functions as a pro-inflammatory factor induced by HFD, and liver-derived ANGPTL8 interacts with the receptor LILRB2 on the membranes of hepatic stellate cells to activate downstream ERK signaling and increase expression of known liver fibrosis genes.
- The serum ANGPTL8 level may represent a potential diagnostic marker for liver fibrosis, and targeting ANGPTL8/LILRB2/ERK signaling holds great promise for developing innovative therapies to treat liver fibrosis.
- Metformin can potentially confer protective effects against the pathological progression known to lead to liver fibrosis in vulnerable patient populations.

GRAPHICAL ABSTRACT

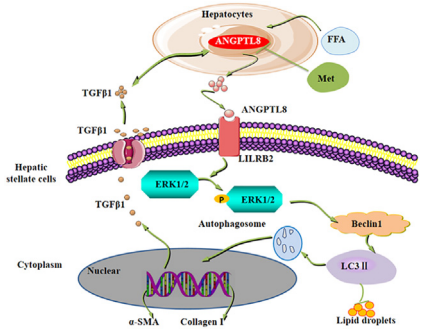

Abbreviations: NAFLD, nonalcoholic fatty liver disease; NASH, nonalcoholic steatohepatitis; HCC, hepatocellular carcinoma; HFD, high fat diets; HFHC, high-fat, high-cholesterol diet; Met, metformin; rANGPTL8, recombinant protein of human ANGPTL8; KO, knockout; LSM, liver stiffness measurement; NCD, normal chow diet; OA, oleic acid.

Peer review under responsibility of Cairo University.

* Corresponding authors at: Institute of Pediatric Disease, Hubei Key Laboratory of Embryonic Stem Cell Research, Taihe Hospital, Hubei University of Medicine, Shiyan, Hubei 442000, China (X. Ruan and X. Guo) Guangdong Engineering & Technology Research Center for Disease-Model Animals, Laboratory Animal Center, Zhongshan School of Medicine, Sun Yat-sen University, Guangzhou 510080, Guangdong, China (W. Cai).

E-mail addresses: caiwb@mail.sysu.edu.cn (W. Cai), ruanxuzhi@163.com (X. Ruan), gxrdl@hbmu.edu.cn (X. Guo).

[1] These authors have contributed equally to this work.

https://doi.org/10.1016/j.jare.2022.08.006

ARTICLE INFO

Article history:
Received 11 April 2022
Revised 24 July 2022
Accepted 8 August 2022
Available online 27 August 2022

Keywords:
Liver fibrosis
HFD
ANGPTL8
Inflammatory activity
LILRB2/ERK signaling pathways

ABSTRACT

Introduction: High calorie intake is known to induce nonalcoholic fatty liver disease (NAFLD) by promoting chronic inflammation. However, the mechanisms are poorly understood.
Objectives: This study examined the roles of ANGPTL8 in the regulation of NAFLD-associated liver fibrosis progression induced by high fat diet (HFD)-mediated inflammation.
Methods: The ANGPTL8 concentration was measured in serum samples from liver cancer and liver cirrhosis patients. *ANGPTL8* knockout(KO) mice were used to induce disease models (HFD, HFHC and CCl4) followed by pathological staining, western blot and immunohistochemistry. Hydrodynamic injection of an adeno-associated virus 8 (AAV8) was used to establish a model for restoring ANGPTL8 expression specifically in *ANGPTL8* KO mice livers. RNA-sequencing, protein array, Co-IP, etc. were used to study ANGPTL8′s mechanisms in regulating liver fibrosis progression, and drug screening was used to identify an effective inhibitor of *ANGPTL8* expression.
Results: ANGPTL8 level is associated with liver fibrogenesis in both cirrhosis and hepatocellular carcinoma patients. Mouse studies demonstrated that ANGPTL8 deficiency suppresses HFD-stimulated inflammatory activity, hepatic steatosis and liver fibrosis. The AAV-mediated restoration of liver ANGPTL8 expression indicated that liver-derived ANGPTL8 accelerates HFD-induced liver fibrosis. Liver-derived ANGPTL8, as a proinflammatory factor, activates HSCs (hepatic stellate cells) by interacting with the LILRB2 receptor to induce ERK signaling and increase the expression of genes that promote liver fibrosis. The FDA-approved anti-diabetic drug metformin, an ANGPTL8 inhibitor, inhibited HFD-induced liver fibrosis in vivo.
Conclusions: Our data support that ANGPTL8 is a proinflammatory factor that accelerates NAFLD-associated liver fibrosis induced by HFD. The serum ANGPTL8 level may be a potential and specific diagnostic marker for liver fibrosis, and targeting ANGPTL8 holds great promise for developing innovative therapies to treat NAFLD-associated liver fibrosis.

Introduction

Nonalcoholic fatty liver disease (NAFLD) is a series of diseases, including hepatocellular steatosis, nonalcoholic steatohepatitis (NASH), fibrosis, cirrhosis and hepatocellular carcinoma (HCC)[1]. NAFLD- associated liver fibrosis is the world's most prevalent chronic liver disease [2], and its incidence rate is increasing year-by-year along with improvements in global living standards. Caloric excess, particularly high fat diets (HFD), has been linked to inflammatory diseases, including NAFLD-associated liver fibrosis [3–5]. Preventing the progression of liver fibrosis can block the occurrence of NAFLD related liver cirrhosis and even HCC [6]. The activation of hepatic stellate cells by inflammation is a marker event of liver fibrosis [7,8]. However, the mechanisms through which caloric excess, such as HFD intake, modulates inflammation are poorly understood.

ANGPTL8, also known as Lipasin, RIFL, or TD26 [9,10,11], is a secretory protein that is highly expressed in the liver, during eating but expressed at low levels during fasting periods [9,12]. ANGPTL8 is an atypical member of the angiopoietin-like family, since it appears to lack a fibrinogen-like domain and does not have the typical coiled-coil domain [9]. These structural features of ANGPTL8 suggest that its function is likely different from other angiopoietin-like proteins. Several recent studies have shown that the circulation level of ANGPTL8 was increased in a NAFLD mouse model and human patients, and showed that ANGPTL8 expression in hepatocytes was induced by HFD [13,14]. Vatner *et al.* found that an antisense oligonucleotide against ANGPTL8 prevented hepatic insulin resistance and steatosis in HFD-fed rats [15]. Approximately 25 % of patients with hepatic steatosis developed into steatohepatitis, and 26 % - 37 % of patients with steatohepatitis develop into liver fibrosis and cirrhosis [16]. Although, studies have observed that serum ANGPTL8 is increased in patients with NAFLD-associated liver fibrosis [17], the function of ANGPTL8 in the etiopathogenesis of NAFLD-associated liver fibrosis is still unknown.

Here we demonstrate that ANGPTL8 functions as a proinflammatory factor and contributes to the progression of NAFLD-associated liver fibrosis induced by HFD, Following our clinical data which suggested that the serum ANGPTL8 level represents a potential diagnostic marker for multiple diseases featuring liver fibrosis, we conducted extensive in vitro and in vivo experiments with diverse research objects, including HSCs and HFD-models induced with *ANGPTL8* KO mice. We characterized the specific roles of liver-derived ANGPTL8 in driving liver fibrosis based on the stimulation of the LILRB2 receptor on HSCs, thereby triggering ERK signaling and HSC activation. Drug screening and subsequent in vivo therapeutic evaluation of the FDA-approved anti-diabetic drug metformin showed that ANGPTL8 can be understood as a vulnerable target for the treatment of liver fibrosis.

Materials and methods

Patient samples

This study was performed with approval from the Ethics Committee at the Affiliated Hospital of Hubei University of Medicine (Taihe Hospital). Serum samples were obtained from healthy volunteers (N = 58), patients with hepatocirrhosis (N = 51) and patients with HCC (N = 51). Patient information is presented in Fig. 1C. Informed written consent was obtained from all subjects.

Mice

ANGPTL8$^{-/-}$(*ANGPTL8* KO) mice were generated in C57BL/6J mice by the CRISPR/Cas9 system using a previously described method in the Laboratory Animal Center of Sun Yat-sen University [18]. We designed three sgRNAs that were cloned into a pX330 plasmid. The sgRNA target sequences are shown in Supplementary Fig S1A. Cas9 mRNA and *ANGPTL8* sgRNA were co-injected into one-cell embryos, and female mice were generated for the F0 generation. The genotyping of transgenic mice in the F1 generation was analyzed by DNA sequencing. All the F0 and F1 generation mice were bred at the Laboratory Animal Center of Sun Yat-sen University, and then the F1 generation mice identified as *ANGPTL8* KO heterozy-

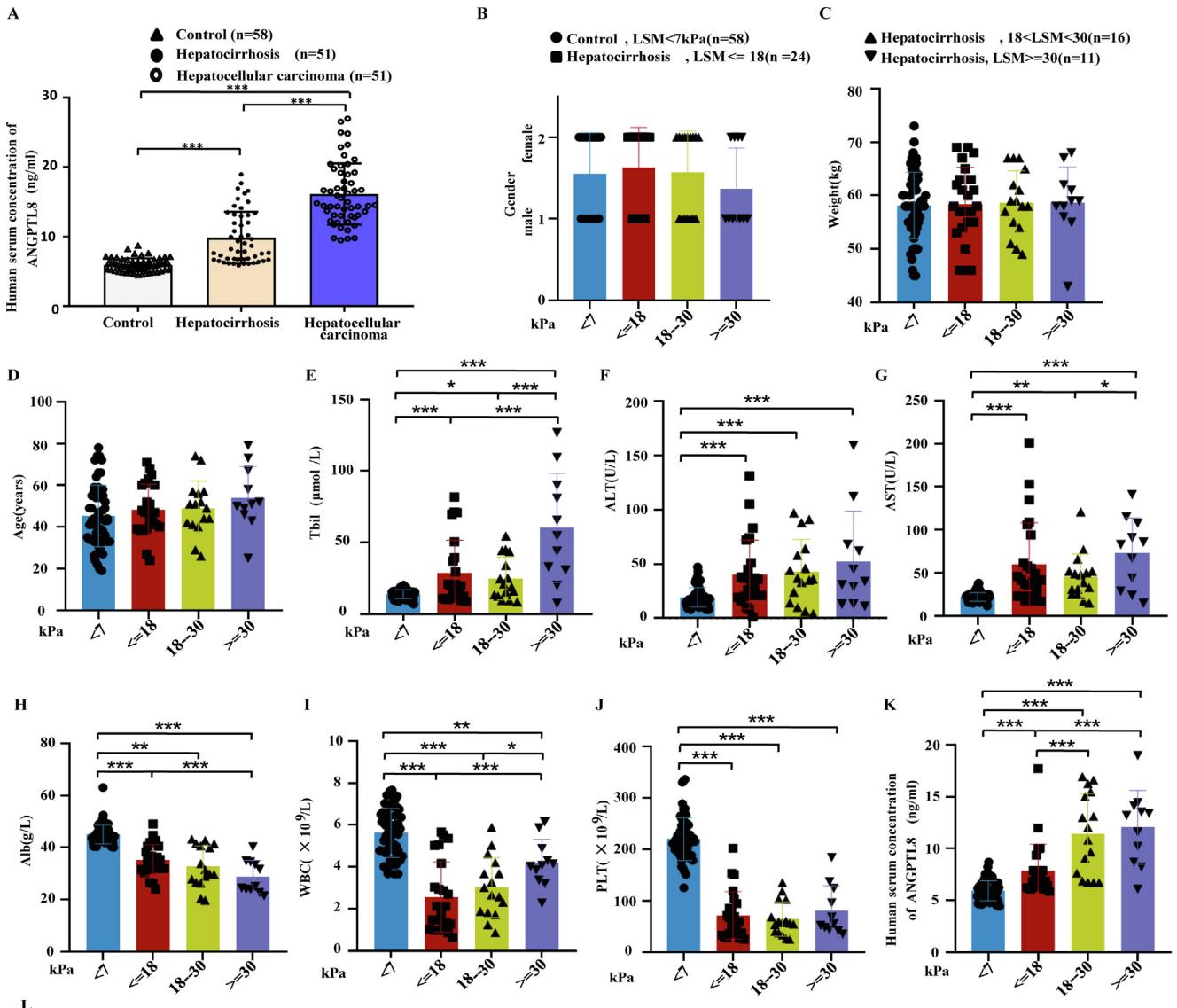

L

Characteristic	Control LSM<7kPa (n=58)	LSM<=18kPa (n=24)	18<LSM<30kPa(n=16)	LSM>=30kPa(n=11)	P value
Age,years	45.28 （19--78）	48.25 （24--71）	49.06 （26--74）	53.9 （25--79）	0.266
Gender,male,n(%)	27(44.83)	9(37.5)	7(43.75)	7(63.64)	0.562
Weight, kg	58.14(45 --73)	58.33(46 --69)	58.69(49 --67)	58.73(43 --68)	0.986
TBIL(umol/L)	13.94 （7.2--20.2）	28.68 （8.8-81.9）	24.84 （8.7--54.5）	60.35 （7.7-126.8）	<0.001 ***
ALT,U/L	19.33 （8--47）	40.38 （1--131）	42.93 （4--97）	52.45 （11--159）	0.005 **
AST,U/L	22.12 （12--38）	60.13 （17--201）	45.69 （15--121）	73 （15--141）	<0.001 ***
ALB,g/L	44.98 （40--63）	35.17 （24--49）	32.72 （19.7--43.2）	28.74 （21.5--40.3）	<0.001 ***
WBC, î 10^9	5.66 （3.67--8.79）	2.56(0.64 --5.66)	3.03(0.87 --5.89)	4.20(2.29 --6.15)	<0.001 ***
PLT, î 10^9	220.05 （125--336）	71.11 （25.6--202）	64.125 （25--135）	80.45 （35--184）	<0.001 ***
ANGPTL8,ng/ml	5.93 （4.43--8.70）	7.83 （6.16--17.70）	11.4 （6.69--16.93）	12.04 （6.10--18.96）	<0.001 ***

Fig. 1. Clinical significance of ANGPTL8 in patients with cirrhosis. (A) ANGPTL8 concentration in the serum of healthy volunteers (control), patients with hepatic-fibrosis (hepatocirrhosis), and patients with hepatocellular carcinoma. ***$p < 0.001$ (one-way ANOVA). (B-L) Cirrhotic patients were divided into three different categories according to their LSM (liver stiffness measurement) as assessed by vibration-controlled transient elastography (FibroScan). Patient characteristics, such as sex, weight, age and serum concentrations of Tbil, ALT, AST, Alb, WBC, PLT, and ANGPTL8 in different groups of patients. *$p < 0.05$, **$p < 0.01$, ***$p < 0.001$ (one-way ANOVA).

gotes were transferred to the SPF Animal Experimental Center of Hubei University of Medicine for further experimental study.

Mice (three to five per cage) were placed in a controlled environment (12 h dark/12 h light cycle, 60–70 % humidity, 23 ± 1 °C). Six- to eight-week- old male C57BL/6J wild type as control mice or *ANGPTL8* KO mice (all the mice were strictly littermates and cohoused) were fed with high-fat diet (HFD; D12492; Research Diets) for different weeks, and a high-fat,

high-cholesterol diet (HFHC; TP26304; Trophic Diets, Nantong, China) for 20 weeks, with a normal chow diet (NCD; D12450J; Research Diets) as a control. We investigated the impact of ANGPTL8 on liver steatosis, inflammation and fibrosis using in vivo experiments with *ANGPTL8* KO mice fed a HFD for up to 28 or 36 weeks [19–21], or HFHC diet for up to 20 weeks [21].

WT and *ANGPTL8* KO mice were divided into a therapeutic group and a PBS group (control group). Metformin (Met) was dissolved in PBS. Mice received Met (200 mg kg-1 i.g.) or PBS administration every day for 4 weeks after 24 weeks of HFD-diet-induced liver fibrosis.

Compliance with ethics requirements

All experiments involving human tissues were conducted according to the ethical policies and procedures approved by the ethics committee of Taihe Hospital, China. The ethical committee number for the study is 201916.

All experiments involving animals were conducted according to the ethical policies and procedures approved by the ethics committee of Hubei University of Medicine, China. The ethical committee number for the study is 202016.

Cells and culture conditions

The HepG2 and LX2 cell lines were purchased from the American Type Culture Collection (ATCC, Manassas, VA, USA) in our study. rANGPTL8 (recombinant protein of human ANGPTL8) was purchased from Novoprotein company and was used to treat cells at a concentration of 500 ng/ml.

Histological analysis

Hematoxylin and eosin (H&E) staining was performed on thin slices that were embedded in a wax block of liver tissue. The overall characteristics of the tissue were observed under a low-power microscope, and then the images of representative areas were observed and collected. The activity score of NAFLD was calculated according to the standard described by Kleiner et al [22]. Histological fibrosis was detected by Masson's and Sirius red staining. The positive area was quantified using ImageJ.

Immunohistochemical staining

All steps of sample processing were performed as described in our previous study [23]. Five-micrometer serial sections were dewaxed in xylene and rehydrated through graded alcohols. Endogenous peroxidases were blocked with H_2O_2 (3 %) for 30 min. Then, they were placed into a microwave oven to repair antigens for 10–15 min at 90–98 °C, cooled at room temperature, and blocked with goat serum for 30 min (nonspecific epitopes were blocked with 5 % normal goat serum; 1:10, Zymed antibody diluent). Then primary antibodies(The antibodies used for immunohistochemistry are listed in Supplementary Table 2) were diluted in 3 %BSA for overnight incubation at 4℃ (use the optimal concentration of antibody explored in the pre-experiment: α-SMA 1:200; Collage I 1:100; F4/80 1:50, as a negative control, an unrelated primary antibody was used). And secondary antibodies (HRP-conjugated, at room temperature) followed by the Liquid DAB Substrate Chromogen System. Two pathologists who were blinded to the information examined all the immunostained sections. Five-seven randomly selected fields of view at a magnification of 100×(100 μm), 200×(50 μm) and 400×(20 μm) were observed respectly. Olympus microscope was used to image the slices. Positive area was quantified using Image J.

q-PCR

Total RNA was extracted and detected according to the instructions of the Invitrogen kit. Reverse transcription was performed using the Superscript II kit for RT-PCR (Tiangen Biotech). The primers for q-PCR are listed in Supplementary Table 1. Fold changes were calculated using the delta–delta Ct method. Three biological replicates at least were performed for all experiments.

Hydrodynamic tail vein injection

ANGPTL8 KO male mice (six to eight weeks old) were used for hydrodynamic tail vein injection, following all details described previously [24].

Fluorescence image analysis

The cells cultured on the glass bottom culture dish were fixed with paraformaldehyde, and then incubated with primary antibody overnight and secondary antibody in a dark environment for 90 min after blocking. Finally, the cells were photographed under a laser confocal microscope (Olympus Japan). We used a lyso-ID red probe to evaluate lysosome content in cells, as the fluorescence intensity will be enhanced under acidic conditions. To quantify acidic autophagic vesicles, cells were transfected with mCherry-GFP-LC3B adenovirus. After rANGPTL8 protein treatment, the percentage of acidic aggregates (red dots/total dots) per cell was counted. Fluorescence images were quantified using ImageJ software.

Western blot analysis

The proteins were extracted by RIPA buffer separated by SDS-PAGE, and then transferred to PVDF membranes. The cells were incubated with blocking buffer (5 % BSA) at room temperature for 1 h and then incubated with antibodies against ANGPTL8, Flag, GAPDH, β-Tubulin, TGFβ1, NF-κB, Smad2/3, LC3, ERK1/2, p-NF-κB, p-ERK1/2, IL-1β, IL-6, p-Smad2/3, Collagen-I, α-SMA, LILRB2, F4/80 and Vimentin (The antibodies used for western blot are listed in Supplementary Table 2.) at 4C overnight or RT for 2 h. The secondary antibody conjugated with horseradish peroxidase was incubated at room temperature for 2 h, Finally, the membranes were incubated in chromogenic reagents A and B and shaken gently at room temperature for 1 min.

Immunofluorescence

Following the method of previous studies with some addition [21,24], the cells were fixed and blocked, and incubated with the following antibodies at 4 ℃ overnight: α-SMA (1:200); Collagen I (1:200); Desmin (1:200); TGFβ1 (1:200). (The antibodies used for immunofluorescence are listed in Supplementary Table 2) . The cells were incubated with the following secondary antibodies for 1 h: FITC-labeled goat anti-rabbit IgG (H + L (1:500)). Nuclei were stained with DAPI for 3 min.

Co-IP assay

LX2 Con cells or *ANGPTL8* OE cells at 80–90 % confluency were lysed in Buffer A (containing 25 mM Tris-HCl, 10 % glycerol, and 150 mM NaCl, and 1 % Triton X-100, pH 7.6) in 6-well plates. Precleared lysates were collected and subjected to protein A + G beads according to the instruction and operation manual.

Cytokine measurements

The ANGPTL8 concentration in the serum supernatant was determined with an ELISA kit (EIAAB Science Inc., China). The linear range of the assay was 78–5000 pg/mL. No significant cross-reactivity or interference was observed.

Cytokine chip detection

We followed the method of previous studies with some addition [25]. Mouse inflammatory cytokine antibody arrays (GSM-INF-1, Ray Biotech Inc.) were used according to the instruction and operation manual. Mouse serum were obtained from different groups for chip detection (Shanghai Kangcheng Bioengineering Co. ltd).

Oil Red O staining

The cells were washed with PBS 3 times, fixed with paraformaldehyde for 15 min, and dyed with Oil Red O solution for 10–30 min. Then, the excess dye solution was washed with 60 % isopropanol and washed three times with distilled water. Mayer's hematoxylin was counterstained for 5–10 min, and 1 % hydrochloric acid was used for color separation and back blue. Three to five independent microscopic fields per well were observed, and images were taken under an inverted microscope.

Primary mouse hepatic stellate cell and hepatocyte isolation

The procedure was performed to a previous study [26,27]. First, the mouse livers were perfused with collagenase (type IV, 100 CDU/ML, Sigma, USA) as liver perfusion reagents, and the liver was excised rapidly and placed into cold HBSS. The primary hepatic cells were released and filtered by a sterile 70-μm filter (Beyotime; FSTR070), and then centrifuged for 5 min at 4 °C at 50 g. The hepatocytes were in the pellet and the HSCs were in the supernatant. Resuspend the hepatocytes in 20 mL of DMEM (HyClone, Germany) containing 10 % FBS for primary hepatocyte culture. The supernatant was centrifuged at 4 ℃ at 400 g, and then the cell precipitate was resuspended in DMEM. The cell suspension was slowly layered on a Percoll gradient (50 %, 35 %, 25 % Percoll) and centrifuged for 20 min at 4℃ at 2000 rpm. White cell rings were carefully collected from the interface and centrifuged at 4 °C for 10 min at 2000 rpm. HSCs were resuspended in DMEM(containing 20 % FBS), resuspended and then seeded into culture dishes.

Measurement of intracellular and hepatic TG content

For intracellular TG content, the cells were fixed, and Oil Red O was extracted. Then, the extracted cells were diluted in 100 % isopropanol and checked at 490 nm using a microplate reader.

For hepatic triglyceride content: lipids were extracted according to a previous study [28]. Lipids were measured using an EnzyChrom™ Triglyceride Assay Kit (BioAssay Systems) and normalized to wet tissue weight.

Statistical analysis

All numeral results are presented as dot plots or means ± SDs. Differences in group results were compared using unpaired two-tailed Student's *t* test or ANOVA. All statistical analyses were performed with GraphPad (Version 8.0) and SPSS (version 19.0). A p value < 0.05 was considered to be a statistically significant.

Results

The ANGPTL8 expression level is correlated with liver fibrosis staging

To evaluate whether *ANGPTL8* expression is associated with liver fibrosis/cirrhosis, we first measured the ANGPTL8 levels in the serum of patients with liver cirrhosis. The serum concentrations of ANGPTL8 increased 1.57 fold in liver cirrhosis patients and 2.14 fold in HCC patients compared to the control (healthy individuals) (Fig. 1A). Furthermore, we found that the highest serum ANGPTL8 level was detected in patients with the most advanced extent of HCC disease progression (Fig. 1A).

We next evaluated whether the serum concentrations of ANGPTL8 could be used as a new diagnostic marker for liver fibrosis. Cirrhotic patients were divided into three different categories according to their liver stiffness measurement (LSM) evaluated by vibration-controlled transient elastography (7 kPa < LSM $\leq$ 18 kPa, 18 kPa < LSM < 30 kPa, and LSM $\geq$ 30 kPa groups); we also defined a "healthy" group based on detected values of LSM < 7 kPa. Our correlation analysis results indicated that the severity of liver cirrhosis was not closely associated with patient characteristics, such as sex, weight, or age (Fig. 1-B-D). Serum analysis demonstrated that Tbil (total bilirubin), ALT (alanine aminotransferase), and AST (aspartate transaminase) levels in the serum of all three cirrhotic patient groups were markedly increased compared to the defined control (healthy group) (Fig. 1E-G). Furthermore, the three cirrhotic patient groups also showed significant decreases in serum albumin content as well as white blood cell and blood platelet counts (Fig. 1H-J). It was also notable that significant decreases in serum albumin content were detected in each of the successively more severe liver cirrhosis patient groups (*i.e.*, decreased albumin upon increased LSM). In direct contrast, the serum ANGPTL8 level significantly increased with increased LSM (Fig. 1K).

Then, we analyzed whether the above indicators could be used as clinical and laboratory diagnostic indicators of liver cirrhosis. As shown in Fig. 1L, Tbil, ALT, AST, Alb, WBC, and PLT could be used as evaluation indexes of liver cirrhosis, which was consistent with previous reports [6]. Our results suggest that the increase lever of ANGPTL8 in serum is associated with liver fibrosis and indicate that the plasma concentrations of ANGPTL8 may be a potentially informative non-invasive biomarker for liver fibrosis.

ANGPTL8 deficiency suppresses HFD-induced hepatic steatosis

We found that HFD could increase the expression of m*ANGPTL8* in mouse liver compared to NCD after feeding (Fig. 2A), and it is known that HFD is a major risk factor for NAFLD [14]. As indicated in Fig. 2B-D, we found that the highest and most important fatty acid components of the HFD unsaturated fatty acids (oleic acid, OA) significantly upregulated the expression of *ANGPTL8* in human liver cells (HepG2), mouse liver cells (H22) and mouse primary hepatocyte cells.

To explore the function of ANGPTL8 in the development of NAFLD, we first investigated the impact of ANGPTL8 on hepatic steatosis using in vivo experiments. After confirming successful CRISPR/Cas9 deletion based generation of F2 *ANGPTL8* KO mice (Fig. S1), both 8-week-old WT and *ANGPTL8* KO mice were given HFD and sacrificed after 28 or 36 weeks. There were no obvious difference in liver appearance between *ANGPTL8* KO and WT mice after 28 and 36 weeks of NCD. After 36 weeks of HFD, the appearance difference of fatty liver between the two groups was obvious (Fig. 2E&F). H&E staining of liver from both the 28 and 36 week groups indicated that fat vacuoles in liver tissue were fewer in the *ANGPTL8* KO group compared to the WT mice, and

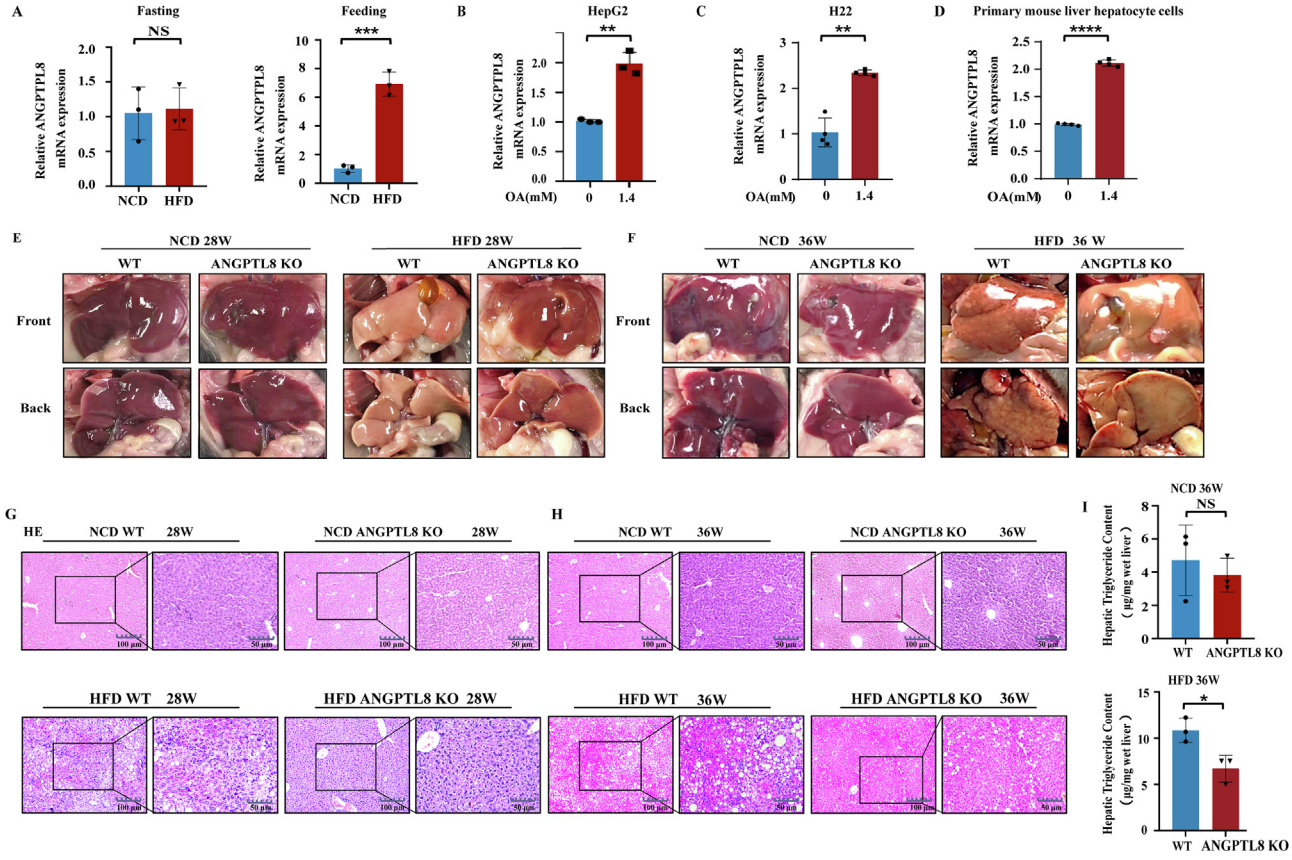

Fig. 2. ANGPTL8 deficiency suppresses HFD-induced hepatic steatosis. (A) The mRNA expression of *ANGPTL8* in the liver of mice induced by NCD (normal chow diet) and HFD (high fatty diet) (left is fasting, right is feeding, n = 3 per group). ***$p < 0.001$ (Student's *t*-test). (B-D) The mRNA expression of *ANGPTL8* in HepG2 (B), H22 (C) and primary mouse liver hepatocytes (D) treated with the fatty acid oleic acid (OA), **$p < 0.01$, ****$p < 0.0001$(Student's *t*-test). (E&F) Hepatic steatosis was confirmed by macroscopic examination in *ANGPTL8* KO or control mice (WT) given with NCD or HFD for 28 (E) or 36 weeks (F), n = 8 per group. (G&H) Hepatic steatosis was confirmed by H&E staining in *ANGPTL8* KO or control mice (WT) given NCD or HFD for 28 or 36 weeks, (n = 8 per group), Scale bars, 100 μm and 50 μm for H&E staining. (I) Quantitative analysis of Hepatic TG in *ANGPTL8* KO and WT mice treated with NCD or HFD 36 weeks (upper is NCD, lower is HFD, n = 3 per group). *$p < 0.05$(Student's *t*-test).

the difference was significantly larger for the 36 week HFD *ANGPTL8* KO group compared to the 28 week group (Fig. 2G&H). The results of quantitative analysis of TG in liver tissue showed that the extent of lipid deposition in the liver tissue was obviously reduced in the *ANGPTL8* KO group compared to the WT mice (Fig. 2I). Collectively, these findings suggest that *ANGPTL8* deficiency suppresses HFD induced hepatic steatosis.

Liver-derived ANGPTL8 accelerates NAFLD-associated liver fibrosis induced by HFD

To investigate whether ANGPTL8 is somehow involved in hepatic fibrosis, we also conducted Masson and Sirius Red staining with the aforementioned HFD-fed mice. Both the 28 and 36 week HFD *ANGPTL8* KO mice displayed dramatically attenuated fibrosis compared to their WT littermates (Fig. 3A&B). Especially after 36 weeks of HFD feeding, the degree of liver fibrosis in WT mice was more significant (approximately 2 fold higher) than that in *ANGPTL8* KO mice. Hepatic F4/80 immunostaining confirmed macrophage infiltration in both genotypes of HFD-fed mice, but the extent of this infiltration was significantly higher in control than that in *ANGPTL8* KO mice (Fig. 3A&B). Staining of liver sections for α-SMA and Collagen I also indicated that the degree of liver fibrosis was attenuated in *ANGPTL8* KO mice. Finally, western blot also indicated that the expression of fibrotic markers was significantly higher in the 36 week HFD WT group (Fig. 3C&D).

The role of ANGPTL8 was also tested in other models of hepatic fibrosis induced by HFHC and CCL4. HFHC can promote the development of NAFLD and accelerate the transition from simple steatosis to non-alcoholic steatohepatitis (NASH). After 20 weeks of HFHC feeding, the liver appearance and HE staining showed that the liver of WT mice was swollen, gray yellow or gray, greasy and formed a large number of fat vacuoles (Fig. S2). Compared to HFHC-induced *ANGPTL8* KO mice, control mice had significant differential expression of various fibrogenic and inflammatory markers (Collagen I, α-SMA and F4/80) in the liver, indicating that ANGPTL8 promoted the formation of hepatic steatosis and fibrosis induced by HFHC (Fig. S2). Compared to CCL4-induced WT mice, *ANGPTL8* KO alleviated CCL4-induced liver fibrosis (Fig. S3). These results indicate that *ANGPTL8* KO could inhibit HFD-, HFHC- and CCL4- induced liver fibrosis, and the difference induced by HFD was the most significant.

We next determined whether liver-specific expression of ANGPTL8 contributes to the process of HFD-induced liver fibrosis. First, we established a model for long-term complementation of liver expression of ANGPTL8 in *ANGPTL8* KO mice by hydrodynamic tail vein injected AAV8. These mice were subsequently fed HFD for 36 weeks, and AAV virus was injection of twice, once every 18 weeks. Compared to *ANGPTL8* KO mice injected with control AAV8, animals complemented with liver expression of ANGPTL8 displayed dramatically increased fibrosis as measured by western blot for fibrogenic markers (Fig. 3D). Collectively, these results show that ANGPTL8 expression in the liver accelerates NAFLD-associated liver fibrosis induced by HFD.

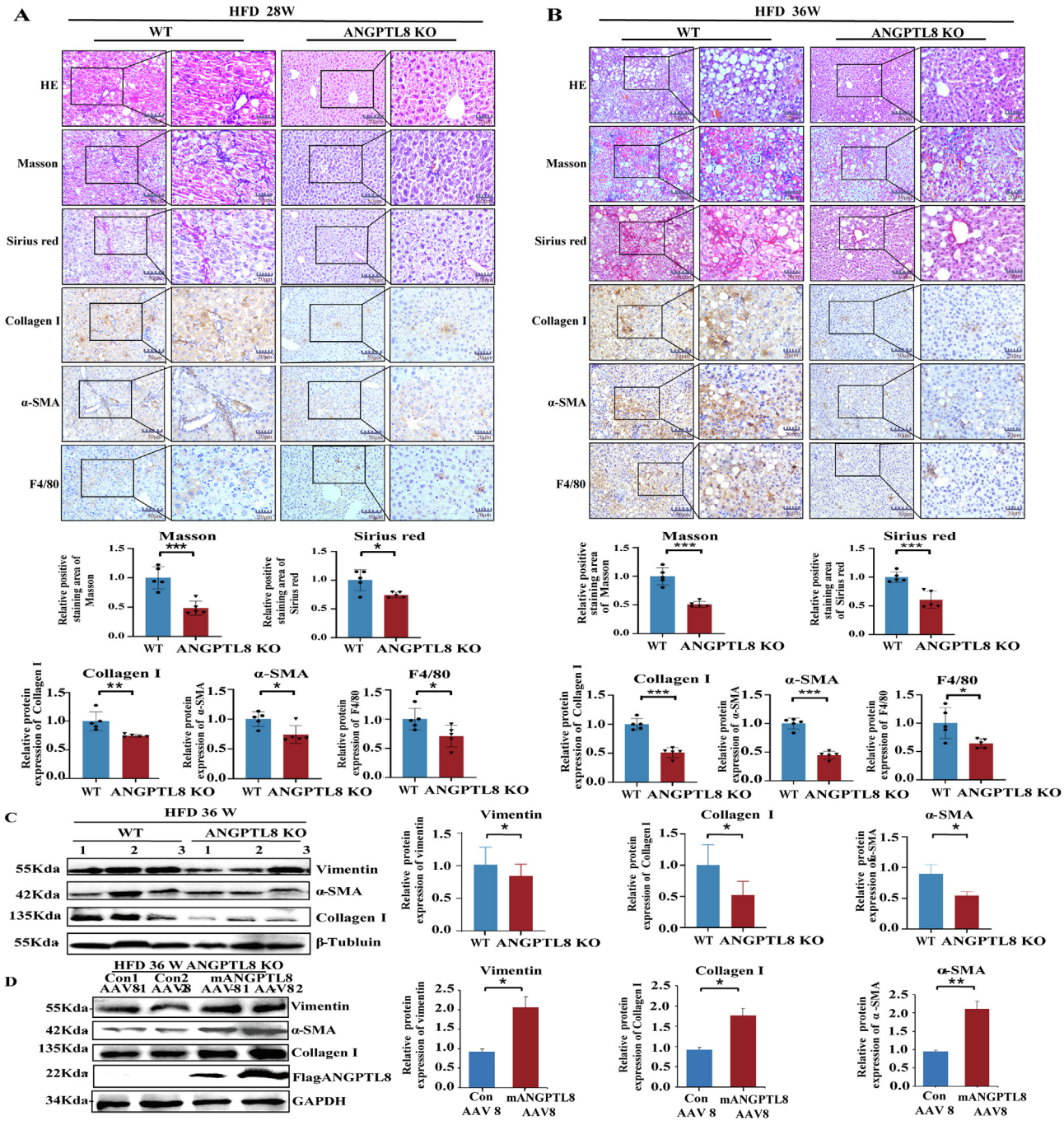

Fig. 3. ANGPTL8 deficiency attenuates HFD-induced liver fibrosis. (A) Liver fibrosis was evaluated by H&E staining, Masson, Sirius red staining, and IHC for the fibrosis markers (α-SMA, Collagen I) and macrophage activation markers (F4/80). Scale bars, 50 μm and 20 μm for H&E staining, Sirius red staining and IHC in *ANGPTL8* KO or control mice (WT) given HFD for 28 weeks. Masson and Sirius red staining, and IHC for α-SMA, Collagen I, and F4/80 (above). Five images of each liver and five livers from different mice were quantified for each group (below), n = 5 per group. $^{*}p < 0.05$, $^{**}p < 0.01$, $^{***}p < 0.001$(Student's *t*-test). (B) Liver fibrosis was evaluated by H&E staining, Masson, Sirius red staining and IHC for α-SMA, Collagen I, and F4/80. Scale bars, 50 μm and 20 μm for H&E staining, Sirius red staining and IHC in *ANGPTL8* KO or control mice (WT) given HFD for 36 weeks. The Masson, Sirius red staining and IHC for α-SMA, Collagen-I, and F4/80 positive liver fibrosis were measured (above). Five images of each liver and five livers from different mice were quantified for each group (below), n = 5 per group. $^{*}p < 0.05$, $^{***}p < 0.001$(Student's *t*-test). (C) The protein levels of α-SMA, Collagen I, and vimentin were determined by western blot in *ANGPTL8* KO or control mice (WT) treated with HFD for 24 weeks. β-Tubulin was used as an internal control (left). Protein expression was normalized to that of β-Tubulin (right), n = 3 per group. $^{*}p < 0.05$(Student's *t*-test). (D) The protein expression of α-SMA, Collagen I and vimentin protein was determined by western blot in *ANGPTL8* KO or control mice (WT) given HFD for 36 weeks. GAPDH was used as an internal control (left). Protein expression was normalized to that of GAPDH (right), n = 4 per group. Mean ± SEM. $^{*}p < 0.05$, $^{**}p < 0.01$(Student's *t*-test). (For interpretation of the references to color in this figure legend, the reader is referred to the web version of this article.)

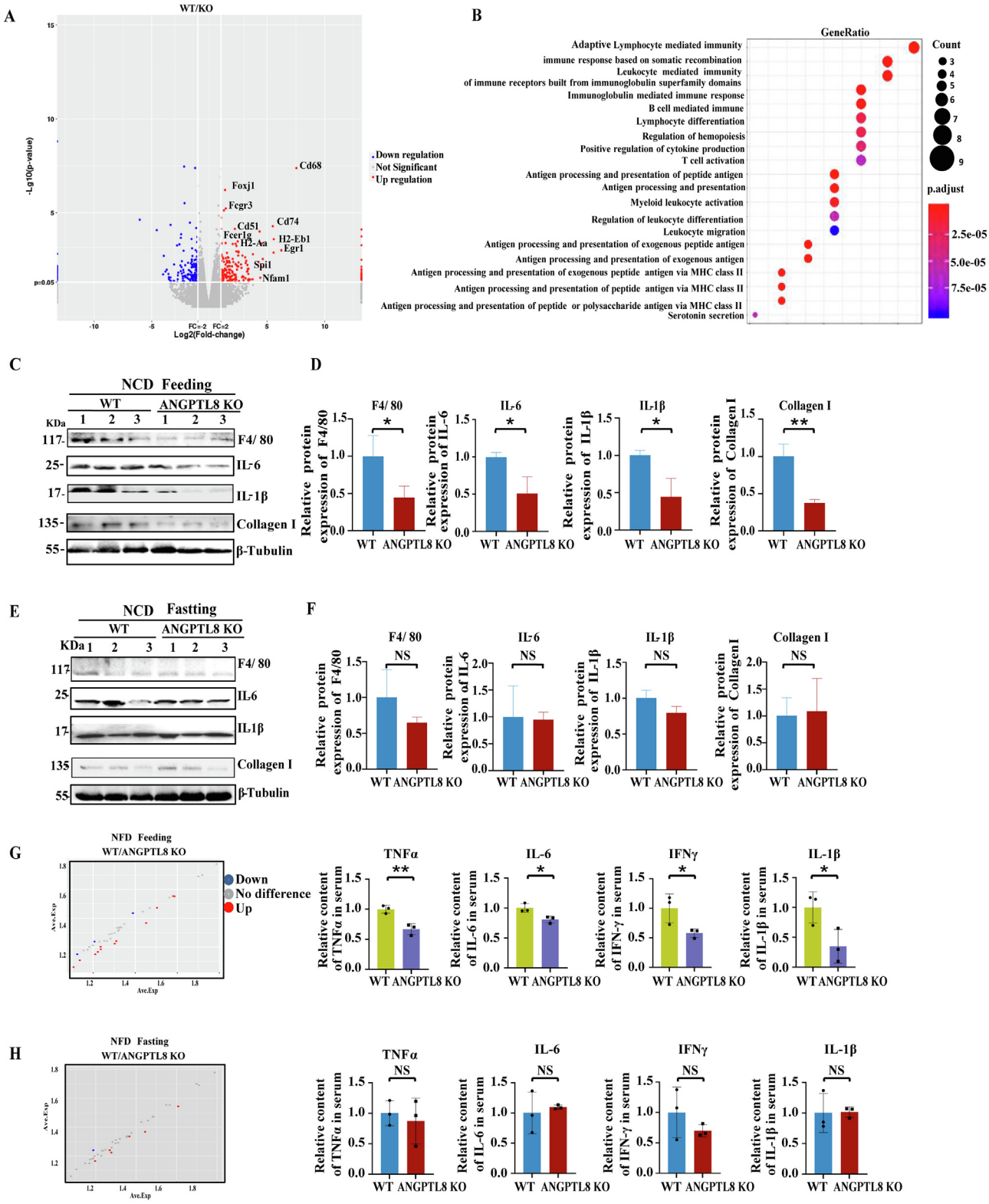

Fig. 4. *ANGPTL8* knockout inhibits HFD-stimulated inflammatory activity in mice. (A) Volcano plot analysis of the RNA sequencing results for the indicated samples. Stringent set ($p < 0.05$) of hepatic genes in HFD-fed *ANGPTL8* KO mice compared with HFD-fed WT mice (n = 3, per group). (B) GO analysis of the RNA sequencing results between the two groups. (C&D) The protein levels of F4/80, IL-6, IL-1β, and Collagen I were determined by western blot of protein extracts from the livers of *ANGPTL8* KO or control mice (WT) after fasting and treated for 12 h with NCD (n = 3). (C) β-Tubulin was used as an internal control. Protein expression was normalized to that of β-Tubulin (D). $^{*}p < 0.05$, $^{**}p < 0.01$(Student's *t*-test). (E&F) The protein levels of F4/80, IL-6, IL-1β, and Collagen I in the livers of *ANGPTL8* KO or control (WT) mice after 2 h feeding with NCD were determined by western blot. (E). β-Tubulin was used as an internal control. Protein expression was normalized to that of β-Tubulin (F). n = 3 per group. (G&H) Mouse inflammatory cytokine antibody array (protein chip, GSM-INF-1, Ray Biotech Inc.) detection of inflammatory factors in the serum of *ANGPTL8* KO or control (WT) mice fed with HFD for 36 weeks after feeding (mice after 2 h's feeding with HFD) (G) and fasting (mice after fasting treated 12 h with HFD) (H) (n = 3 per group). $^{*}p < 0.05$, $^{**}p < 0.01$ (Student's *t*-test).

Feeding-stimulated high expression of ANGPTL8 controls HFD-induced inflammatory activity in mice

To explore the mechanism(s) underlying how *ANGPTL8* KO suppresses HFD-induced hepatic fibrosis, we performed RNA-seq analysis of livers dissected from WT and *ANGPTL8* KO mice treated with HFD for 36 weeks. Heat-map analysis highlighted obvious differences (>2 fold) in the gene expression profiles of WT mice vs *ANGPTL8* KO mice, and ingenuity pathway analysis annotated the molecular and cellular functions of the differentially expressed genes (using a $p < 0.05$ cutoff) (Fig. 4A). The top-ranking disease-associated pathway for these genes was "inflammatory response" (Fig. 4B). The differentially expressed genes included genes known to function in lymphocyte-mediated immune responses, including B lymphocyte mediated immune related genes and T lymphocyte mediated immune related genes (Fig. 4A-B).

ANGPTL8 is a secretory protein with high expression after feeding [29], so we also performed western blot to measure any differences in the accumulation levels of inflammatory factors in liver samples of *ANGPTL8* KO and WT mice under both fasting and feeding factors. Among the NCD groups, the livers of the *ANGPTL8* KO mice had significantly reduced accumulation of the inflammatory factors IL-1β, IL-6, and F4/80 compared to the livers of WT mice (Fig. 4C&D). However, there was no significant change between WT and *ANGPTL8* KO mice after fasting (Fig. 4E&F). These results suggest that ANGPTL8 regulates postprandial inflammatory responses.

To investigate how ANGPTL8 regulates HFD-induced inflammation, we collected sera from WT and *ANGPTL8* KO mice fed with HFD for 36 weeks and conducted protein chip analysis of both fasting and feeding samples to examine the levels of inflammatory factor. Among the HFD-fed groups, upon feeding, the serum concentrations of IL-6, TNF-α, IL-1β, and IFN-γ were significantly lower in the *ANGPTL8* KO mice than that in the WT mice (Fig. 4G). However, there was no significant difference between WT and *ANGPTL8* KO mice after fasting (Fig. 4H). We also used western blot with antibodies against IL-1β and IL-6 to analyze the liver tissues from the HFHC-fed (20 week) animals and found that the levels of these hepatic inflammatory factors were significantly elevated in WT mice compared to *ANGPTL8* KO mice (Fig. S4A). These results show that ANGPTL8 promotes the accumulation of hepatic inflammatory factors, and this was further supported by our observation of significantly elevated liver IL-6 and IL-1β levels upon AAV8-mediated complementation of ANGPTL8 expression in the livers of *ANGPTL8* KO mice fed with HFD (Fig. S4B).

Meanwhile, the results of RNA-seq showed that the most significantly different genes were enriched in the TGFβ signaling pathway (Fig. S5A), and *ANGPTL8* KO could regulate TGFβ1 expression in mouse liver and mouse liver hepatocyte cells (Fig. S5B&C). As shown in Fig. S5 (D&E), the addition of ANGPTL8 protein (rANGPTL8) to the growth media of mouse liver hepatocyte cells significantly enhanced the protein and mRNA expression of the inflammatory factor TGFβ1. *ANGPTL8* OE or K_D regulated TGFβ1 expression in HepG2 cells (Fig. S5F). As shown in Fig. S5 (G&H), the addition of OA to the growth media of HepG2 cells significantly enhanced the expression of the inflammatory factor TGFβ1 (Fig. S5G). The addition recombinant TGFβ1 protein to the media significantly increased the transcription of *ANGPTL8* (Fig. S5H). Moreover, the addition of fatty-acid (OA) to the media significantly increased the transcription of TGFβ1 in WT mouse liver hepatocytes. However, TGFβ1 did not change after OA stimulation in *ANGPTL8* KO mouse liver hepatocyte cells (Fig. S5I). Based on the sequencing results, we found significant differences in the expression of transcription factors SPI1/PU.1, which regulates TGFβ1 by enrichment analysis of the sequencing results [30,31]. Western blot results also further demonstrated that *ANGPTL8* KO could significantly reduce SPI1 expression in the livers of mice treated with HFD for 36 weeks (Fig. S5J). These experiments clearly revealed that ANGPTL8 regulates TGFβ1 via a positive feedback mechanism, suggesting that ANGPTL8 may act as a proinflammatory factor.

ANGPTL8 as a proinflammatory factor directly activates HSCs by binding to the receptor LILRB2

HSCs can promote liver fibrosis upon stimulation with various inflammatory stimuli [7]. Because HSCs do not express *ANGPTL8* (Fig. S6), we speculated that excess lipids may stimulate hepatic parenchymal cells to express and secrete ANGPTL8, which may activate HSCs directly; alternatively, secreted ANGPTL8 could indirectly activate HSCs by inducing hepatic cells to secrete other factors that promote hepatic fibrosis (Fig. 5A).

To analyze whether ANGPTL8 activates HSCs, we first stimulated cultured HSCs (LX2 cell line) with human ANGPTL8 recombinant protein (rANGPTL8, 500 ng/ml). Strikingly, addition of rANGPTL8 to the HSC media or exogenous ANGPTL8 protein (*ANGPTL8*-OE) strongly induced fibrogenesis. *ANGPTL8*-OE promoted two classic HSC activation phenotypes: the transformation of HSCs to myofibroblast-like cells (Fig. S7A), and reduced lipid accumulation (Fig. 5B). Interestingly, ANGPTL8 induced the expression of α-SMA, Collagen I, and TGFβ1, with the strongest induction observed at the 2-hour time point during an 18-hour incubation time course (Fig. 5C). We then shortened the stimulation times to 0, 0.5, 1, and 2 h, and found that the expression of all three proteins peaked at 0.5 h (Fig. 5D). *ANGPTL8*-OE also upregulated α-SMA, Collagen I, and TGFβ1 expression in LX2 cells (Fig. 5E). We also verified the effects of rANGPTL8 on the activation of isolated mouse primary hepatic stellate cells by immunofluorescence, and the result showed that the expression levels of Desmin, α-SMA, Collagen I, and TGFβ1 were increased significantly (Fig. 5F). Thus, we preliminarily confirmed that ANGPTL8 promotes the activation of hepatic stellate cells.

Given that ANGPTL8 is a secreted protein and is not expressed in mouse primary HSCs or human LX2 cells, we investigated potential ANGPTL8 receptors on the cell membranes of HSCs. Previous studies have shown that LILRB2 (the human immune inhibitory receptor leukocyte immunoglobulin-like receptor B2) and PirB (its mouse ortholog paired immunoglobulin-like receptor), are receptors for several angiopoietin-like proteins [32,33]. Therefore, we speculated that LILRB2 is a potential receptor for ANGPTL8 in HSCs. First, Co-IP (co-immunoprecipitation) assays indicated that these two proteins undergo a physical interaction (Fig. 5G, Fig S7B). Then we found that ANGPTL8 could up-regulate the expression of LILRB2 in LX2 cells (Fig. 5H-J). We also found that stimulation of LX2 cells with rANGPTL8 rapidly and significantly upregulated the expression of α-SMA, Collagen I and TGFβ1, and this induction was blocked when an anti-LILRB2 antibody was used to pretreat the LX2 cells prior to rANGPTL8 stimulation (Fig. 5K). All the results support that ANGPTL8, as a proinflammatory factor, directly activates HSCs by binding to the receptor LILRB2.

ANGPTL8-induced HSC activation via the LILRB2/ERK signaling pathway modulates autophagy

To obtain further insights into the role of LILRB2 in hepatic fibrosis induced by ANGPTL8, we examined the livers of *ANGPTL8* KO mice after 36 weeks of HFD feeding, and specifically focused on the activating phosphorylation of two kinases known to be regulated by LILRB2/PirB: ERK1/2, NF-κB and other signaling pathways. As shown in Fig. 6A and Fig. S8, *ANGPTL8* KO significantly decreased the levels of p-ERK1/2 and p-NF-κB, but did not regulate p-FAK and p-Smad2/3 expression. The same pattern of kinase acti-

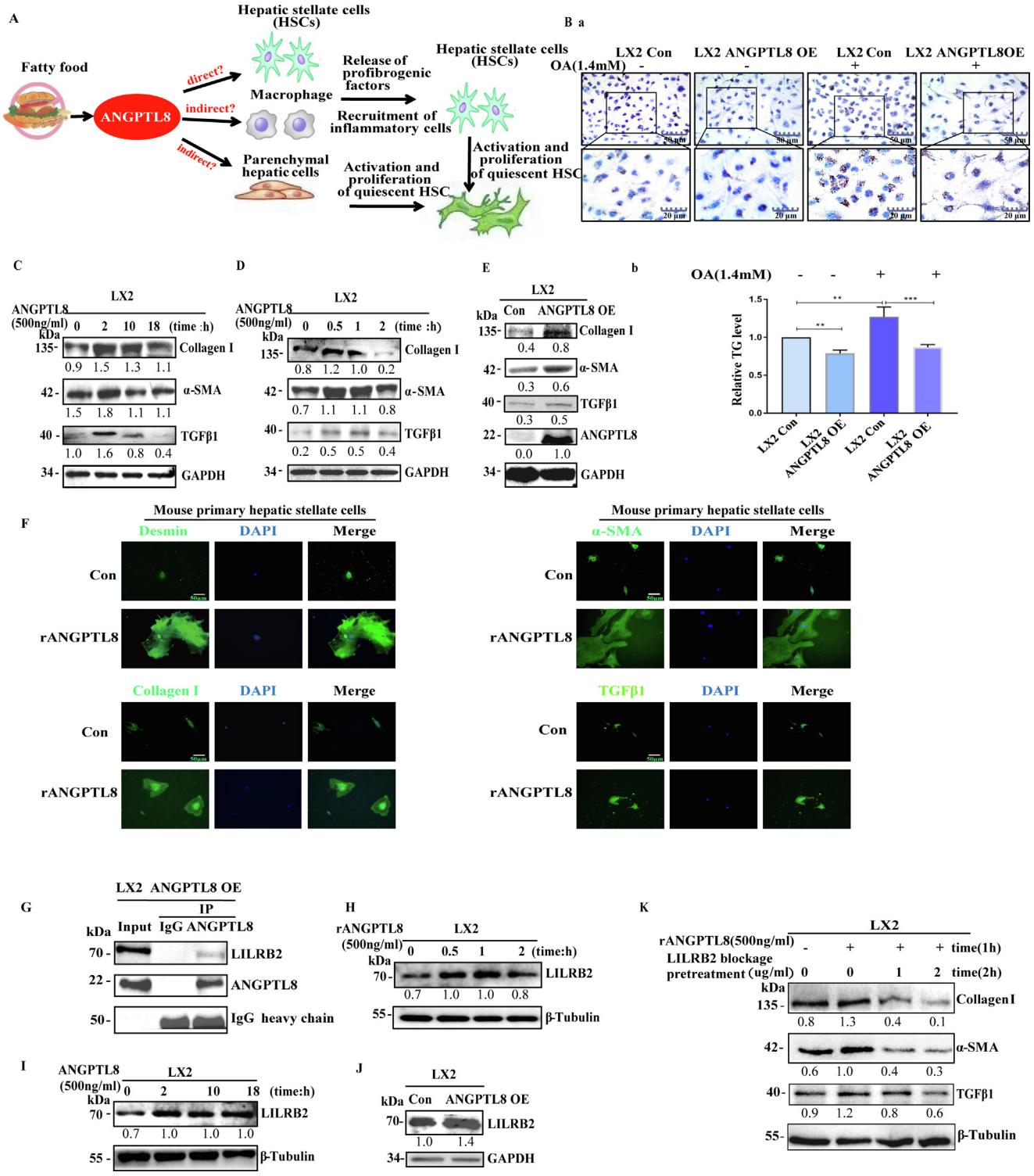

Fig. 5. ANGPTL8 directly activates HSCs by interacting with the receptor LILRB2 on hepatic stellate cells. (A) Conceptual model for ANGPTL8-mediated activation of hepatic stellate cells. (B) Representative images of oil red O staining (a) and intracellular TG levels (b) in *ANGPTL8* OE and control LX2 cells. scale bar: 50 μm and 20 μm. (C-E) Western blot analysis of rANGPTL8- (C&D) and *ANGPTL8* OE- (E) induced protein changes of Collagen I, α-SMA, and TGFβ1 in LX2 cells, the ratio to GAPDH is shown in the middle as numbers, and the numbers represent the average of 3 independent experiments. (F) Immunofluorescence detection of Desmin, α-SMA, Collagen I and TGFβ1 in mouse primary hepatic stellate cells induced by ANGPTL8 recombinant protein. The mouse primary hepatic stellate cells were fixed and stained with antibodies Desmin, α-SMA, Collagen I, TGFβ 1 and visualized with secondary antibody. Microphotographs were taken with a fluorescence microscope. scale bar:50 μm. (G) Immunoprecipitation examination of the interaction between ANGPTL8 and LILRB2. The Co-IP experiment was performed using anti-ANGPTL8 antibody in LX2 cell lysates and then analyzed by western blot with anti-ANGPTL8 and anti-LILRB2 antibodies. The negative control was IgG. (H-J) Western blot analysis of *ANGPTL8* OE (J) and rANGPTL8 (H&I) induced protein changes in LILRB2 in LX2 cells. The ratio to GAPDH or β-tubulin is shown in the middle as numbers, and the numbers represent the average of 3 independent experiments. (K) Exogenous ANGPTL8-induced expression of α-SMA and Collagen I was inhibited upon antibody blocking of LILRB2 in LX2 cells. The ratio to β-tubulin is shown in the middle as numbers, and the numbers represent the average of 3 independent experiments. (For interpretation of the references to color in this figure legend, the reader is referred to the web version of this article.)

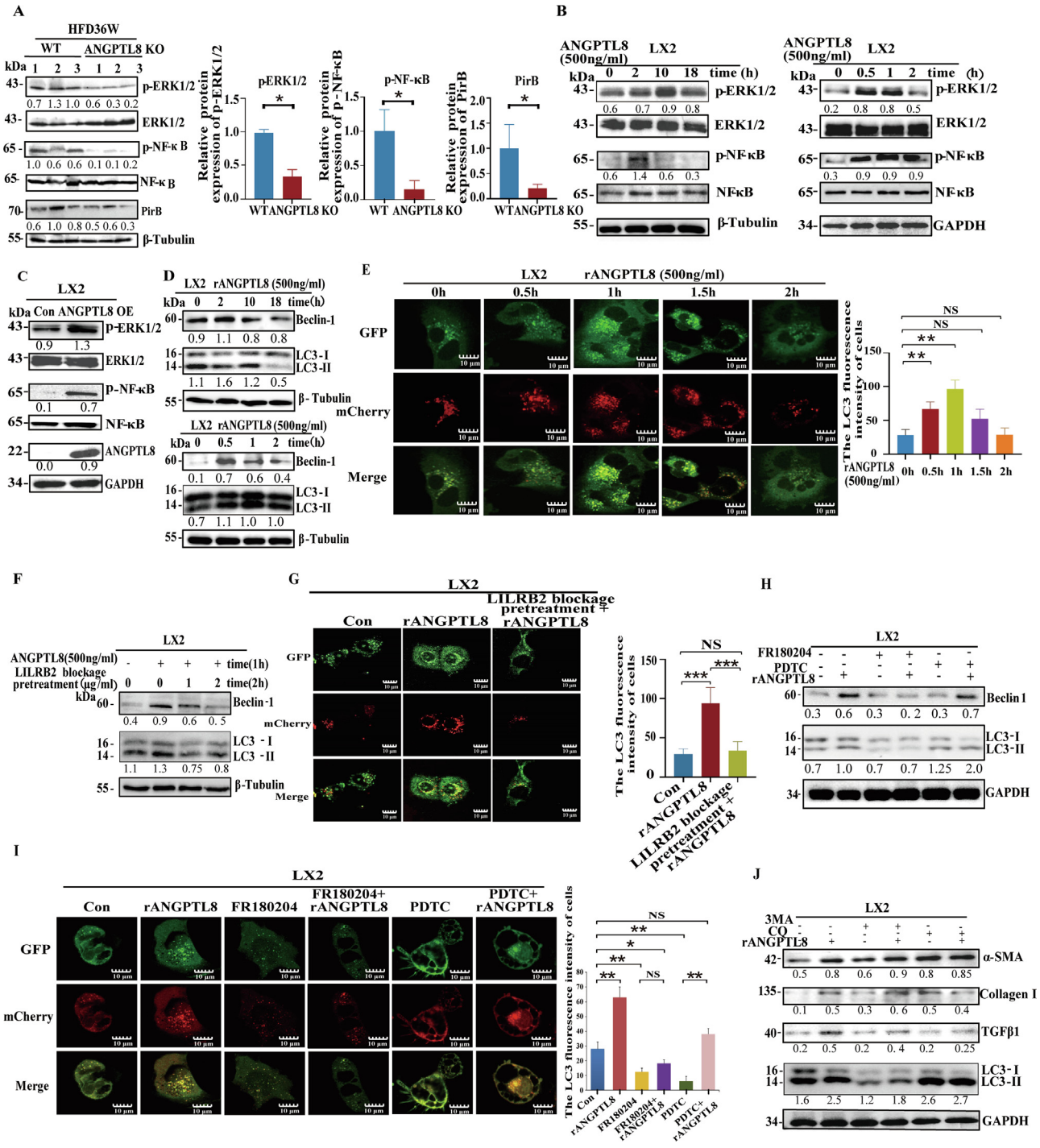

Fig. 6. ANGPTL8-induced HSC activation by LILRB2/ERK signaling modulates autophagy. (A) The protein levels of ERK1/2, p-ERK1/2, NF-κB, p-NF-κB, and PirB were determined by western blot of extracts from the livers of *ANGPTL8* KO and control mice (WT) mice given HFD for 36 weeks. The ratio to β-tubulin is shown in the middle as numbers, and the numbers represent the average of 3 independent experiments. $^{*}p < 0.05$(Student's *t*-test). (B&C) The protein levels of ERK1/2, p-ERK1/2, NF-κB, and p-NF-κB were determined by western blot in LX2 cells treated with rANGPTL8 (B) and *ANGPTL8* OE (C). The ratio to GAPDH or β-tubulin is shown in the middle as numbers, and the numbers represent the average of 3 independent experiments. (D&E) ANGPTL8 activates the autophagy process by interacting with LILRB2. The protein levels of LC3-II/LC3-I and Beclin-1 were determined by western blot in LX2 cells treated with exogenous ANGPTL8 protein. The ratio to β-tubulin or LC3-II/LC3-I is shown in the middle as numbers, and the numbers represent the average of 3 independent experiments (D). mRFP-GFP-LC3 expression lentivirus was used to infect LX2 cells for 24 h, then the cells were treated with ANGPTL8 protein for 0–2 h, and fluorescence images were captured(E). Scale bar: 10 μm,$^{**}p < 0.01$(one-way ANOVA). (F&G) Blocking LILRB2 with an antibody inhibited rANGPTL8-induced expression of LC3-II/LC3-I and Beclin-1 in LX2 cells, the ratio to β-tubulin or LC3-II/LC3-I is shown in the middle as numbers, and the numbers represent the average of 3 independent experiments (F). LX2 cells were infected with mRFP-GFP-LC3 expression lentivirus for 24 h, and pretreated with LILRB2 antibody for 2 h. Then, the cells were treated with ANGPTL8 protein for 1 h, and fluorescence images were captured (G). Scale bar:10 μm,$^{***}p < 0.001$(one-way ANOVA). (H-J) Analysis of ANGPTL8′s function in activating autophagy by up-regulating phosphorylation of ERK downstream of LILRB2. FR180204 (ERK inhibitor) and PDTC (NF-κB inhibitor) were used to treat LX2 cells to analyze whether ANGPTL8 activates astrocyte autophagy by upregulating ERK or NF-κB protein phosphorylation by western blot. (H) mRFP-GFP-LC3 expression lentivirus was infected into LX2 cells for 24 h, and then the cells were treated with the inhibitors FR180204 or PDTC for 24 h, followed by rANGPTL8 protein for 1 h; fluorescence images were captured for cells with ANGPTL8-induced expression of LC3-II/LC3-I (I). Immunoblots of LX2 cell lysates scale bar:10 μm, $^{*}p < 0.05$, $^{**}p < 0.01$(one-way ANOVA). (J) Cells were pretreated with inhibitors (3MA: 20 μM, CQ: 50 μM) for 24 h, and then treated with ANGPTL8 for 1 h. The ratio to GAPDH or LC3-II/LC3-I shown is in the middle as numbers, and the numbers represent the average of 3 independent experiments.

vation was observed upon rANGPTL8 stimulation of LX2 cells. Both endogenous and exogenous ANGPTL8 promoted the phosphorylation levels of ERK and NF-κB (Fig. 6B&C).

Since both ERK and NF-κB signaling can promote fibrosis by regulating autophagy [34,35], we next tested the effect of ANGPTL8 on the expression of key autophagy proteins. rANGPTL8 stimulation of LX2 cells significantly increased the expression of Beclin-1 and LC3-II/LC3-I (Fig. 6D). Furthermore, confocal microscopy results revealed that the ratio of RFP-LC3 puncta to total LC3 punctate structures of the mRFP-GFP-LC3 tandem reporter was increased following rANGPTL8 stimulation (Fig. 6E), showing that ANGPTL8 stimulation of LILRB2 signaling promotes autophagosome formation in HSCs. Consistently, pretreatment of LX2 cells with an anti-LILRB2 antibody blocked rANGPTL8-induced expression of Beclin-1 and LC3-II/LC3-I and reduced the extent of autophagosome formation (Fig. 6F&G). These results indicate that ANGPTL8 is sufficient to activate the autophagy process through its interaction with LILRB2.

We then examined autophagy-related signaling events downstream of ANGPTL8-LILRB2 binding. Assays showed that the presence of an ERK inhibitor (FR180204) abrogated ANGPTL8-induced expression of LC3-II/LC3-I in rANGPTL8-simulated LX2 cells. In contrast, LC3-II/LC3-I levels were unchanged in the presence of the NF-κB inhibitor PDTC (Fig. 6H&I). These results implicate ERK signaling in ANGPTL8′s activation of autophagy. Additional assays using two classic autophagy inhibitors (3MA and CQ) [35,36] showed that ANGPTL8′s activation of autophagy involves impairment of autophagosome fusion with lysosomes rather than obviously disrupting PI3K signaling (Fig. 6J). These findings collectively support that the binding of ANGPTL8 with LILRB2 at the surface of HSCs induces fibrogenesis by activating ERK signaling-mediated autophagy.

Screening of ANGPTL8 inhibitors and evaluation of therapeutic effects on NAFLD-associated liver fibrosis

Our results confirmed a role for ANGPTL8 in the development of NAFLD, suggesting that inhibiting the expression of ANGPTL8 could be a new strategy for the treatment of HFD-induced NAFLD. Given the known contributions of metabolic disorders to high-fat diet induced liver fibrosis [37], we screened five drugs used clinically for the treatment of glucose and lipid metabolism disorders. *ANGPTL8* mRNA expression was reduced in human HepG2 cells (3.4 fold lower) and in mouse liver (4.1fold lower) upon treatment with the FDA-approved biguanide class drug metformin (Fig. 7A, Fig. S9). Then, we tested the in vivo therapeutic effect of metformin on liver fibrosis in WT and *ANGPTL8* KO mice. The mice were fed a HFD for 24 weeks and then given metformin for 4 weeks while continuing HFD feeding (see the experimental design flow chart in Fig. 7B). The livers of metformin-treated mice were more ruddy and smooth than the livers of PBS control mice (Fig. 7C). Pathological staining analyses showed that metformin inhibited HFD- induced liver fibrosis in WT and *ANGPTL8* KO mice, and the degree of hepatic fibrosis in WT mice in the control PBS and metformin groups was much more severe that than those in *ANGPTL8* KO mice (Fig. 7D).

Recalling our finding that the secretory proinflammatory factor ANGPTL8 could directly activate HSCs, we next explored whether metformin exerts its antifibrotic effect by inhibiting ANGPTL8-mediated activation of HSCs. LX2 cells were treated with metformin, rANGPTL8, or both. We found that metformin inhibited the rANGPTL8-induced morphological transformation of LX2 cells into myofibroblast-like cells (Fig. S10A). Oil red O staining revealed that the number of lipid droplets in rANGPTL8-exposed LX2 cells was significantly lower than that in LX2 control cells. Upon metformin treatment, the number of lipid droplets in the cytoplasm of control cells increased, whereas the rANGPTL8-exposed LX2 cells displayed a much less obvious increase in the number of lipid droplets (Fig. S10B). We also found that stimulation of LX2 cells with metformin rapidly and significantly downregulated the expression of TGFβ1 and α-SMA (Fig. 7E&F). Notably, the addition of rANGPTL8 to the medium did not counteract the effect of metformin.

Discussion

NAFLD contains a range of disorders from simple steatosis to severe forms of liver injury including liver fibrosis and HCC. However, how it induces the progression from steatosis to liver fibrosis is not fully understood [6,38]. Inflammation is one of the key initiating factors of disease transformation [4]. The chronic exposure of liver cells to a caloric excess such as HFD environment, can lead to continuous accumulation of triglycerides and derived toxic metabolites in the liver, thereby activating inflammatory pathways [39,40]. Therefore, recent studies have proposed "intermittent fasting or caloric restriction" and pointed out that fasting can inhibit the "outbreak" of inflammation in the body [41–43]. However, the strict requirements of intermittent fasting or caloric restriction make it difficult for people to persist in it for a long time. Therefore, it is essential to determine the key genes that control caloric excess diet-induced inflammatory activity and whether intervention with these genes could replace the therapeutic effect of intermittent fasting. In our study, we provided several novel findings demonstrating that ANGPTL8 is a key regulator of NAFLD-associated liver fibrosis progression by regulating HFD-induced inflammatory activity.

ANGPTL8 is a newly discovered member of ANGPTLs. As a secretory protein, it is highly expressed in human liver tissue and secreted into the blood after feeding [44]. Many studies suggest that ANGPTL8 is involved in lipid metabolism by increasing serum TG levels [13,14,45]. Hepatic expression of ANGPTL8 was increased in NAFLD mice, including ob/ob or db/db mice, and mice fed with HFD or diet of deficient in methionine-choline [14]. Recent studies have also found that ANGPTL8 plays a role in inflammatory diseases [44,46]. Therefore, we speculate that ANGPTL8 may play a key role in the progression from steatosis to liver fibrosis.

To confirm the above hypothesis, we first analyzed the relationship between the expression of ANGPTL8 and liver fibrosis. Here, we found that up-regulation of ANGPTL8 expression in serum is associated with liver fibrosis in humans. Our results suggest that the increased lever of ANGPTL8 in serum is associated with liver fibrosis and indicate that the serum concentrations of ANGPTL8 may be a potentially informative non-invasive biomarker for liver fibrosis. High fat stimulation can induce strong expression of *ANGPTL8* in human HepG2 cells and mouse liver parenchymal cells. Upon establishment of HFD-, HFHC- and CCL4- induced liver fibrosis models, we observed that knockout of ANGPTL8 inhibited HFD-, HFHC- and CCL4- induced liver fibrosis, and the difference induced by HFD was the most significant. Although, given the known expression of ANGPTL8 is high in liver and adipose tissue [47], Oldoni *et al.* showed that ANGPTL8 from liver and adipose tissue has different roles in the process of lipid metabolism, and their results suggest that hepatic secretion of ANGPTL8 is the main source for its role in regulating lipid metabolism and obesity [48]. This suggests that liver derived ANGPTL8 may regulate hepatic fibrogenesis, so we specifically complemented ANGPTL8 expression in the livers of *ANGPTL8* KO mice and found that liver-derived ANGPTL8 accelerates NAFLD-associated liver fibrosis induced by HFD.

To better understand the basis of previous observations about ANGPTL8 deficiency in suppressing HFD-induced hepatic fibrosis, we performed protein chip and RNA-seq analyses of livers dissected from WT and *ANGPTL8* KO mice fed HFD for 36 weeks. The RNA-seq results demonstrated that genes downregulated in the liver of HFD-fed *ANGPTL8* KO mice were associated with

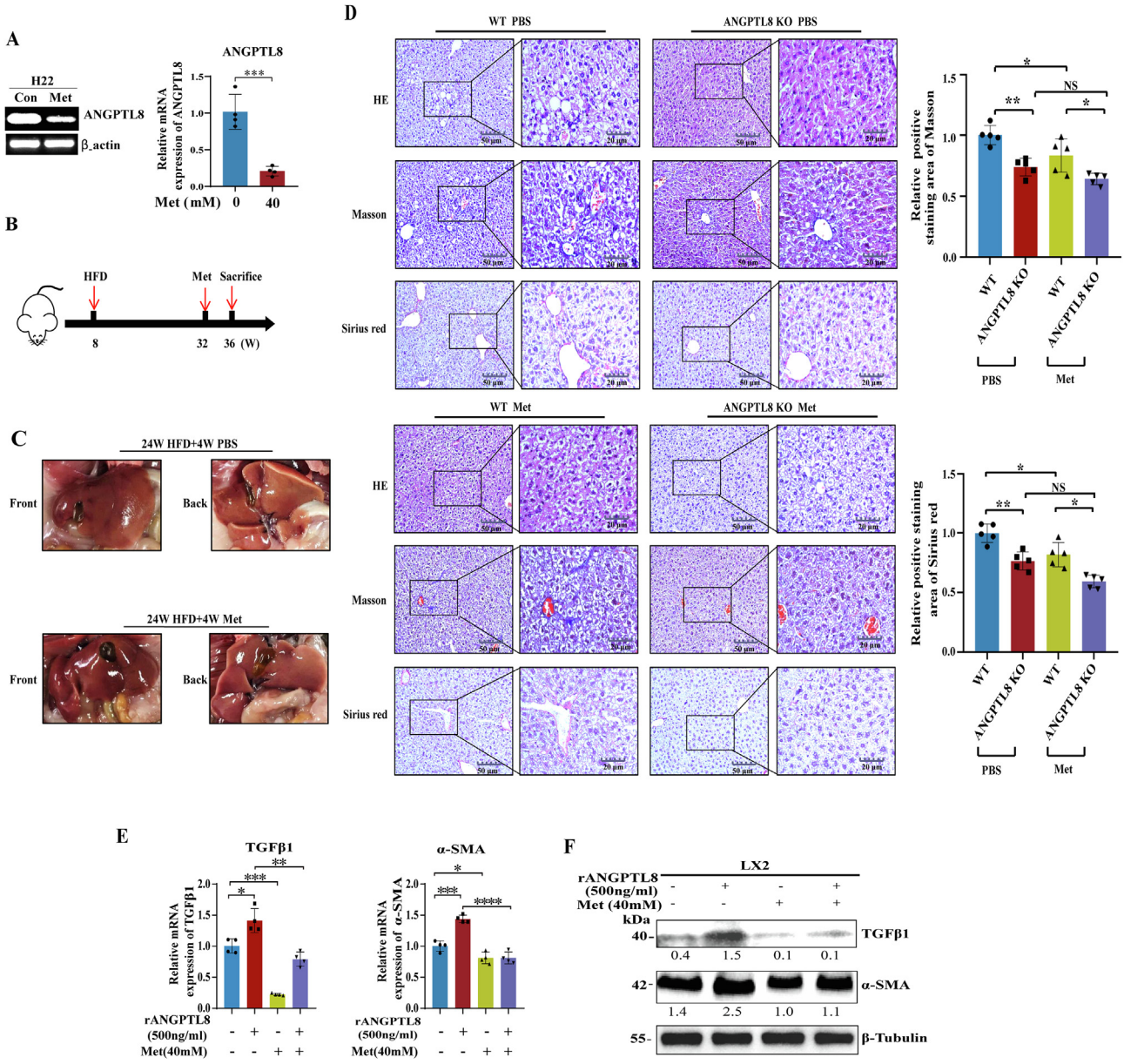

Fig. 7. Effect of metformin on HFD-induced liver fibrosis. (A) Analysis of the effect of metformin (Met) on *ANGPTL8* expression in mouse liver cells by RT-PCR and qPCR. (B) Schematic diagram of Met treatment of HFD-induced liver fibrosis in mice. (C) Macroscopic examination of livers to analyze the potential therapeutic effects of metformin on HFD-induced liver fibrosis in WT mice (n = 6 per group). (D) Level in Met and PBS treated mice (*p < 0.05, n = 6 per group). Liver fibrosis was evaluated by H&E staining, Masson, Sirius red staining and IHC for α-SMA, Collagen I, and F4/80. Scale bars, 50 μm and 20 μm for H&E staining, Sirius red staining and IHC in *ANGPTL8*KO or WT mice given HFD for 24 weeks and treated with Met for 4 weeks. Five images of each liver, and five livers from different mice, were quantified for each group (*p < 0.05, n = 6 per group). (E) The mRNA expression of α-*SMA* and *TGFβ1* was determined by qPCR in LX2 cells treated with metformin and rANGPTL8 for 1 h. (F) The protein levels of α-SMA and TGFβ1, were determined by western blot in LX2 cells treated with metformin and rANGPTL8 for 1 h. (For interpretation of the references to color in this figure legend, the reader is referred to the web version of this article.)

regulatory processes involved in leukocyte activation, immune processes, immune cell differentiation and the TGFβ signaling pathway. Christ et al., also found that systemic inflammation induced by caloric excess (Western Diet) was largely influenced by dietary changes, but innate immune responses induced by myeloid cells remained increased and could potentially promote inflammatory related diseases [49]. Then, we examined the relationship between ANGPTL8, hyperlipidemia and inflammation in both in vitro and in vivo analyses in diverse HFD mouse models. We found that feeding-stimulated high expression of ANGPTL8 controls HFD-induced inflammatory activity and regulates TGFβ1 via a positive feedback mechanism. ANGPTL family proteins such as ANGPTL2 can increase TGFβ1 expression to promote renal fibrosis through α5β1 integrin [50]. However, they did not find TGFβ1′s feedback regulation of ANGPTL2 expression. Therefore, it is very interesting to find that ANGPTL8 regulates TGFβ1 via a positive feedback mechanism, which suggests that ANGPTL8 may act as a proinflammatory factor downstream of TGFβ1. It is noteworthy that TNFα might also be associated with angiogenesis during the injury healing process of the injured liver during the development of liver fibrosis [51]. Our results also showed that upon feeding, the serum concentrations of TNF-α were significantly lower in *ANGPTL8* KO mice than in WT mice, and many studies have shown that TGFβ1 and TNFα can interact with each other to regulate multiple diseases, including liver fibrosis [52]. Our results suggest that ANGPTL8 may serve as a key nexus gene in the reciprocal regulation of TGF-β and TNF-α. However, how ANGPTL8 regulates TGF-β and TNF-α expression needs further study.

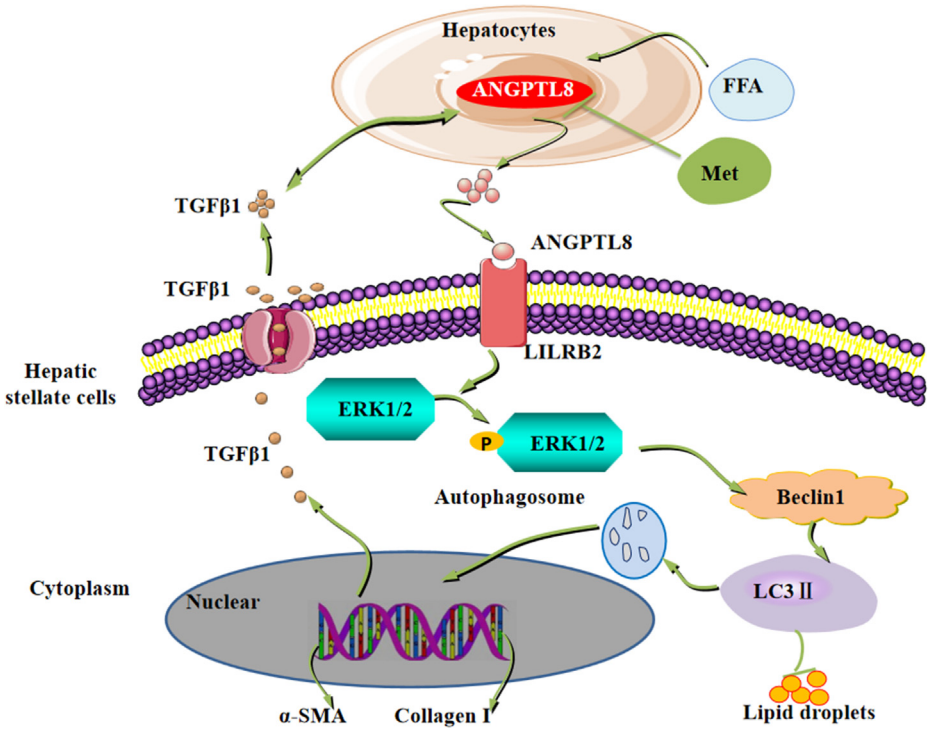

Fig. 8. Schematic representation of the proposed mechanism of ANGPTL8 as an inflammatory factor that promotes HFD-induced NAFLD-associated liver fibrosis by activating LILRB2/ERK signaling in hepatic stellate cells. The elevated fatty acid levels upon long-term exposure to HFD up-regulate liver *ANGPTL8*. ANGPTL8, in turn, functions as a proinflammatory factor promoting the expression and secretion of the inflammatory factor TGFβ1. Secreted TGFβ1 in turn promotes the expression and secretion of ANGPTL8. Secreted ANGPTL8 interacts with the receptor LILRB2 on the membrane of HSCs thereby activating downstream ERK signaling and increasing the expression of known liver fibrosis genes. Metformin can inhibit the expression of *ANGPTL8* and attenuate HFD-induced hepatic fibrosis in mouse livers.

If ANGPTL8 is a proinflammatory factor, how does it affect HSCs to promote liver fibrosis? The progression is promoted by the activation of HSCs by various inflammatory stimuli [53,54]. HSC activation causes the transformation of HSCs into myofibroblast-like cells with excessive collagen production [7]. At the cellular level, our finding that HSCs do not express *ANGPTL8* motivated our hypothesis that a HFD may stimulate *ANGPTL8* expression in hepatic parenchymal cells. Indeed, we found that parenchymal cell-secreted ANGPTL8 can interact with its LILRB2 receptor on HSCs to directly trigger HSC activation. LILRB2 functions as a receptor receptors for several angiopoietin-like proteins [32]. LILRB2, as an immune checkpoint receptor regulates many physiological responses by interacting with diverse ligands [55–57]. Thus, our results confirm that ANGPTL8, as a pro-inflammatory factor, directly induces hepatic fibrosis via LILRB2/ERK signaling-mediated autophagy in HSCs. Although we did not analyze whether ANGPTL8 is a ligand for the LILRB2 receptor, and the critical site (s) at which they interact is not known, the screen identified an interaction between them that provides direction for functional dissection of ANGPTL8.

Our findings linking ANGPTL8 to the development of liver fibrosis suggested that inhibiting ANGPTL8 expression may represent a promising strategy for the treatment of HFD-induced liver fibrosis. We conducted drug screening which revealed that metformin—an FDA-approved biguanide class drug used to treat high blood glucose levels in diabetic patients, which has also been shown to exert other functions [58,59], including anti-tumor and anti-aging effects [58–60]—could inhibit the expression of *ANGPTL8* in human HepG2 cells and mouse liver, and conferred protection against HSC activation in the liver as induced by HFD. It has been reported that metformin has an anti-liver fibrosis effect by improving insulin resistance [61,62], but its specific mechanism is not fully understood, especially in the treatment of NAFLD-associated liver fibrosis. Our results showed that metformin inhibited the mRNA expression of *ANGPTL8*, and amelioration of HFD-induced liver fibrosis was dependent on inhibition of ANGPTL8 expression in vivo. These results again pinpoint ANGPTL8 as a vulnerable target for the treatment of liver fibrosis, and expand the novel uses of metformin.

Conclusion

Our findings ultimately support a model (Fig. 8), wherein fatty acids (FFAs) in HFD up-regulate liver *ANGPTL8* expression, which promotes the expression and secretion of the inflammatory factor TGFβ1. Secreted TGFβ1 in turn promotes the expression of *ANGPTL8*, and secreted ANGPTL8 acts as a proinflammatory factor and directly interacts with the HSC membrane receptor LILRB2 to activate downstream ERK signaling, thereby elevating the expression of fibrogenesis genes in the liver. Excitingly, our study also indicates that the safe and widely used anti-diabetic drug metformin can inhibit the expression of *ANGPTL8*, conferring protection against fibrosis in the livers of wild type HFD-fed mice. In conclusion, our study defines ANGPTL8 as a vulnerable target for protecting liver cells against HFD-induced inflammation and subsequent fibrogenesis. Our results also indicate that the serum ANGPTL8 level represents a potential diagnostic marker for diseases featuring liver fibrosis and suggest that metformin can potentially confer protective effects against the pathological progression known to lead to liver cancer in vulnerable patient populations.

Compliance with Ethics Requirements

Patient samples were performed with approval from the Ethics Committee at the Affiliated Hospital of Hubei University of Medi-

cine. All animal experiments were reviewed and approved by the Institutional Animal Care and Use Committee at the Hubei University of Medicine prior to the initiation of any studies.

Declaration of Competing Interest

The authors declare that they have no known competing financial interests or personal relationships that could have appeared to influence the work reported in this paper.

Acknowledgment

This study was financially supported by the National Natural Science Foundation of China (No. 82073232, 82101632, 81700769, 81641028), the Hubei Science & Technology Department Foundation (2020CFB558, 2018ACA162), the Key Projects of Hubei Education (D20202103), the Department of Biomedical Research Foundation, Hubei University of Medicine (HBMUPI201803), the Innovative Research Program for Graduates of Hubei University of Medicine (YC2020039, YC2020002, YC2019003, YC2019008), the Advantages Discipline Group(medicine) Project in Higher Education of Hubei Province(2022XKQT3, 2022XKQY1) and the Scientific Research Project of Shiyan Science and Technology Bureau (21Y06, 21Y38).

Appendix A. Supplementary material

Supplementary data to this article can be found online at https://doi.org/10.1016/j.jare.2022.08.006.

References

[1] He Y, Hwang S, Cai Y, Kim S, Xu M, Yang D, et al. MicroRNA-223 ameliorates nonalcoholic steatohepatitis and cancer by targeting multiple inflammatory and oncogenic genes in hepatocytes. Hepatology 2019;70(4):1150–67.
[2] Younossi Z, Anstee QM, Marietti M. Global burden of NAFLD and NASH: trends, predictions, risk factors and prevention. Nat Rev Gastroenterol Hepatol 2018;15(1):11–20.
[3] He T, Xu C, Krampe N. High-fat diet exacerbates SIV pathogenesis and accelerates disease progression. J Clin Investig 2019;129(12):5474–88.
[4] Lumeng CN, Saltiel AR. Inflammatory links between obesity and metabolic disease. J Clin Investig 2011;121(6):2111–7.
[5] Kani AH, Alavian SM, Esmaillzadeh A. Effects of a low-calorie, low-carbohydrate soy containing diet on systemic inflammation among patients with nonalcoholic fatty liver disease: a parallel randomized clinical trial. Horm Metab Res 2017;49(9):687–92.
[6] Friedman SL, Neuschwander-Tetri BA, Rinella M, SanyalFriedman AJ. Mechanisms of NAFLD development and therapeutic strategies. Nat Med 2018;24(7):908–22.
[7] Kisseleva T, Cong M, Paik Y. Myofibroblasts revert to an inactive phenotype during regression of liver fibrosis. Proc Natl Acad Sci U S A 2012;109(24):9448–53.
[8] Iwaisako K, Jiang C, Zhang M. Origin of myofibroblasts in the fibrotic liver in mice. Proc Natl Acad Sci U S A 2014;111(32):E3297–305.
[9] Wang Y, Quagliarini F, Gusarova V. Mice lacking ANGPTL8 (Betatrophin) manifest disrupted triglyceride metabolism without impaired glucose homeostasis. Proc Natl Acad Sci U S A 2013;110(40):16109–14.
[10] Fu Z, Berhane F, Fite A. Elevated circulating lipasin/betatrophin in human type 2 diabetes and obesity. Sci Rep 2014;4:5013.
[11] Wang C, Tong Y, Wen Y, Cai J. Hepatocellular carcinoma-associated protein TD26 interacts and enhances sterol regulatory element-binding protein 1 activity to promote tumor cell proliferation and growth. Hepatology 2018;68(5):1833–50.
[12] Dang F, Wu R, Wang P, Wu Y, Azam MS. Fasting and feeding signals control the oscillatory expression of angptl8 to modulate lipid metabolism. Sci Rep 2016;6:36926.
[13] Hong BS, Liu J, Zheng J, Ke W. Angiopoietin-like protein 8/betatrophin correlates with hepatocellular lipid content independent of insulin resistance in non-alcoholic fatty liver disease patients. J Diabetes Investig 2018;9(4):952–8.
[14] Lee Y-H, Lee S-G, Lee CJ. Association between betatrophin/ANGPTL8 and non-alcoholic fatty liver disease: animal and human studies. Sci Rep 2016;6:24013.
[15] Vatner DF, Goedeke L, Camporez J-P-G. Angptl8 antisense oligonucleotide improves adipose lipid metabolism and prevents diet-induced NAFLD and hepatic insulin resistance in rodents. Diabetologia 2018;61(6):1435–46.
[16] Geh D, Manas DM, Reeves HL. Hepatocellular carcinoma in non-alcoholic fatty liver disease-a review of an emerging challenge facing clinicians. Hepatobiliary Surg Nutr 2021;10(1):59–75.
[17] Cengiz M, Ozenirler S, Kocabiyik M. Serum β-trophin level as a new marker for noninvasive assessment of nonalcoholic fatty liver disease and liver fibrosis. Eur J Gastroenterol Hepatol 2016;28(1):57–63.
[18] Huang L, Li G, Ding Y, Sun J, Wu T, Zhao W, et al. LINGO-1 deficiency promotes nerve regeneration through reduction of cell apoptosis, inflammation, and glial scar after spinal cord injury in mice. Exp Neurol 2019;320:112965.
[19] Yu Y, Liu Y, An W, Song J, Zhang Y, Zhao X. STING-mediated inflammation in Kupffer cells contributes to progression of nonalcoholic steatohepatitis. J Clin Investig 2018;129(2):546–55.
[20] Koppen AV, Verschuren L, Hoek A, Verheij J, Morrison MC, Li K, et al. Uncovering a predictive molecular signature for the onset of NASH-Related fibrosis in a translational NASH mouse model. Cell Mol Gastroenterol Hepatol 2018;5(1):83–98.
[21] Ye P, Liu J, Xu W. Dual-specificity phosphatase 26 protects against nonalcoholic fatty liver disease in mice through transforming growth factor beta-activated Kinase 1 suppression. Hepatology 2019;69(5):1946–64.
[22] Kleiner DE, Brunt EM, Natta MV. Design and validation of a histological scoring system for nonalcoholic fatty liver disease. Hepatology 2005;41(6):1313–21.
[23] Guo X, Shan M, Huang Y, Zhang Z, Yuan Y, Meng Z, et al. BARMR1-mediated sorafenib resistance is derived through stem-like property acquisition by activating integrin-FAK signaling pathways. Signal Transduction Targeted Ther 2020;5(1):97.
[24] Zhang Z, Wu H, Dai L, Yuan Y, Zhu Y, Ma Z, et al. ANGPTL8 enhances insulin sensitivity by directly activating insulin-mediated AKT phosphorylation. Gene 2020;749:144707.
[25] Jurisic V. Multiomic analysis of cytokines in immuno-oncology. Expert Rev Proteomics 2020;17(9):663–74.
[26] Marcela A-V, Michaela T, Cecilia M, et al. Isolation of Kupffer cells and hepatocytes from a single mouse liver. Methods Mol Biol 2017;1639:161–71.
[27] Shi W, Wang Y, Zhang C, Jin H, Sun G. Isolation and purification of immune cells from the liver. Int Immunopharmacol 2020;85:106632.
[28] Lytle KA, Bush NC, Triay JM, Kellogg TA, Kendrick ML, Swain JM, *et al.* Hepatic fatty acid balance and hepatic fat content in humans with severe obesity. 2019, 104(12)**:** 6171-6181.
[29] Chi X, Britt EC, Shows HW. ANGPTL8 promotes the ability of ANGPTL3 to bind and inhibit lipoprotein lipase. Mol Metab 2017;6(10):1137–49. S2212877817303307.
[30] Hu J, Zhang J-J, Li L, Wang S, Kong B. PU.1 inhibition attenuates atrial fibrosis and atrial fibrillation vulnerability induced by angiotensin-II by reducing TGF-β1/Smads pathway activation. J Cellular Mol Med 2021;25(14):6746–59.
[31] Liu Q, Yu J, Wang L, Tang Y, Qiang L. Inhibition of PU.1 ameliorates metabolic dysfunction and non-alcoholic steatohepatitis. J J Hepatol 2020;73(2):361–70.
[32] Zheng J, Umikawa M, Cui C. Inhibitory receptors bind ANGPTLs and support blood stem cells and leukaemia development. Nature 2015;485(7400):656–60.
[33] Chen S, Feng M, Zhang S, Dong Z, Wang Y, Zhang W, et al. Angptl8 mediates food-driven resetting of hepatic circadian clock in mice. Nat Commun 2019;10(1):3518.
[34] Day CP, Saksena S. Non-alcoholic steatohepatitis: Definitions and pathogenesis. J Gastroenterol Hepatol 2002;Suppl 3:S377–84.
[35] Verma N, Manna SK. Advanced Glycation End Products (AGE) Potently Induce Autophagy through Activation of RAF Protein Kinase and Nuclear Factor κB (NF-κB). J Biol Chem 2016;291(3):1481–91.
[36] Wang S, Livingston MJ, Su Y, Dong Z. Reciprocal regulation of cilia and autophagy via the MTOR and proteasome pathways. Autophagy 2015;11(4):607–16.
[37] Ibrahim SH, Hirsova P, Gores GJ. Non-alcoholic steatohepatitis pathogenesis: sublethal hepatocyte injury as a driver of liver inflammation. Gut 2018;67(5):963–72.
[38] Samar H, Ibrahim PH. Gregory J Gores Non-alcoholic steatohepatitis pathogenesis: sublethal hepatocyte injury as a driver of liver inflammation. Gut 2018;67(5):963–72.
[39] Choi IY, Lee C, Longo VD. Nutrition and fasting mimicking diets in the prevention and treatment of autoimmune diseases and immunosenescence. Mol Cell Endocrinol 2017;455:4–12.
[40] Jordan S, Navpreet T, Casanova-Acebes M, Christie C, Zhang D. Dietary intake regulates the circulating inflammatory monocyte pool. Cell 2019;178(5):1102–1114.e17.
[41] Marinho TS, Ornellas F, Barbosa-da-Silva S, Mandarim-de-Lacerda CA, Aguila MB. Beneficial effects of intermittent fasting on steatosis and inflammation of the liver in mice fed a high-fat or a high-fructose diet. Nutrition 2019;65:103–12.
[42] Gabandé-Rodríguez E, Heras MMGdl, Mittelbrunn M. Control of inflammation by calorie restriction mimetics: on the crossroad of autophagy and mitochondria. Cells 2019;9(1):82.
[43] Ma S, Sun S, Geng L, Song M, Liu G. Caloric restriction reprograms the single-cell transcriptional landscape of rattus norvegicus aging. Cell 2020;180(5).
[44] Yang Y, Jiao X, Li L, Hu C, Qin Y. Increased circulating angiopoietin-like protein 8 levels are associated with thoracic aortic dissection and higher inflammatory conditions. Cardiovasc Drugs Ther 2020;34(1):65–77.
[45] Guo C, Zhao Z, Deng X, Chen Z, Tu Z, Yuan G. Regulation of angiopoietin-like protein 8 expression under different nutritional and metabolic status. Endocr J 2019;66(12):1039–46.

[46] Liao Z, Wu X, Song YS, Luo R, Yin H, Zhan S, et al. Angiopoietin-like protein 8 expression and association with extracellular matrix metabolism and inflammation during intervertebral disc degeneration. J Cell Mol Med 2019;23(8):5737–50.
[47] Zhang R, Abou-Samra AB. Emerging roles of Lipasin as a critical lipid regulator. Biochem Biophys Res Commun 2013;432(3):401–5.
[48] Oldoni F, Cheng H, Banfi S, Gusarova V, Hobbs HH. ANGPTL8 has both endocrine and autocrine effects on substrate utilization. JCI Insight 2020;5(17):e138777.
[49] Christ A, Günther P, Lauterbach M, Duewell P, Biswas D, Pelka K, et al. Western Diet Triggers NLRP3-Dependent Innate Immune Reprogramming. Cell 2018;172(1–2).
[50] Morinaga J, Kadomatsu T, Miyata K. Angiopoietin-like protein 2 increases renal fibrosis by accelerating transforming growth factor-β signaling in chronic kidney disease. Kidney Int 2016;89(2):327–41.
[51] Jurisic V, Terzic T, Colic S, Jurisic M. The concentration of TNF-alpha correlate with number of inflammatory cells and degree of vascularization in radicular cysts. Oral Dis 2008;14(7):600–5.
[52] Liu ZW, Zhang YM, Zhang LY, Zhou T, Li YY, Zhou GC, et al. Duality of interactions between TGF-beta and TNF-alpha during tumor formation. Front Immunol 2021;12:810286.
[53] Krishnan A, Abdullah TS, Mounajjed T. A longitudinal study of whole body, tissue and cellular physiology in a mouse model of fibrosing NASH with high fidelity to the human condition. Am J Physiol Gastrointest Liver Physiol 2017;312(6):G666–80.
[54] Henao-Mejia J, Elinav E, Jin C, Hao L. Inflammasome-mediated dysbiosis regulates progression of NAFLD and obesity. Nature 2012;482(7384):179–85.
[55] Anderson KJ, Allen RL. Regulation of T-cell immunity by leucocyte immunoglobulin-like receptors: innate immune receptors for self on antigen-presenting cells. Immunology 2009;127(1):8–17.
[56] Chang CC, Ciubotariu R, Manavalan JS, Yuan J, Colovai AI, Piazza F, et al. Tolerization of dendritic cells by T(S) cells: the crucial role of inhibitory receptors ILT3 and ILT4. Nat Immunol 2002;3(3):237–43.
[57] Kuroki K, Matsubara H, Kanda R, Miyashita N, Maenaka K. Structural and functional basis for LILRB immune checkpoint receptor recognition of HLA-G isoforms. J Immunol 2019;203(12):3386–94.
[58] Zhou J, Massey S, Story D, Li L. Metformin: an old drug with new applications. Int J Mol Sci 2018;19(10):2863.
[59] Neumann B, Baror R, Zhao C, Segel M, Dietmann S, Rawji KS, et al. Metformin restores CNS remyelination capacity by rejuvenating aged stem cells. Elsevier Sponsored Documents 2019;25(4):473–85.
[60] Xie J, Xia L, Xiang W, He W, Gao G. Metformin selectively inhibits metastatic colorectal cancer with the KRAS mutation by intracellular accumulation through silencing MATE1. Proc Natl Acad Sci 2020;117(23):13012–22.
[61] Shankaraiah RC, Callegari E, Guerriero P, Rimessi A, Pinton P, Gramantieri L, et al. Metformin prevents liver tumourigenesis by attenuating fibrosis in a transgenic mouse model of hepatocellular carcinoma. Oncogene 2019;38(45):7035–45.
[62] Heeba GH, El-Deen RM, Abdel-Latif RG, Khalifa M. Combined treatments with metformin and phosphodiesterase inhibitors alleviate nonalcoholic fatty liver disease in high-fat diet fed rats: a comparative study. Can J Physiol Pharmacol 2020;98(8):498–505.